Cellulose Nanocrystal-Based Poly(Butylene Adipate-Co-Terephthalate) Nanocomposites Covered With Antimicrobial Silver Thin Films

Filipe V. Ferreira,[1,2] **Marcos Mariano**,[2] **Ivanei F. Pinheiro**,[1] **Elisa M. Cazalini**,[3] **Diego H.S. Souza**,[4] **Laura S.S. Lepesqueur**,[5] **Cristiane Y. Koga-Ito**,[5] **Rubia F. Gouveia**,[2] **Liliane M.F. Lona**[1]

[1]*School of Chemical Engineering, University of Campinas (UNICAMP), Campinas, São Paulo, Brazil*

[2]*Brazilian Nanotechnology National Laboratory (LNNano), Brazilian Center for Research in Energy and Materials (CNPEM), Campinas, São Paulo, Brazil*

[3]*Department of Physics, Technological Institute of Aeronautics (ITA), São José dos Campos, São Paulo, Brazil*

[4]*Institute of Macromolecules Professor Eloísa Mano (IMA), Federal University of Rio de Janeiro (UFRJ), Rio de Janeiro, Brazil*

[5]*Department of Biosciences and Oral Diagnosis, Institute of Science and Technology, São Paulo State University (UNESP), São José dos Campos, São Paulo, Brazil*

In this study, we reported the preparation and prospective application of the nanocomposites of poly(butylene adipate-co-terephthalate) (PBAT) reinforced with cellulose nanocrystals (CNCs). CNCs were isolated from bleached sugarcane bagasse by acid hydrolysis and functionalized with adipic acid. Nanocomposites were prepared with different concentration of CNCs (0.8, 1.5, and 2.3 wt% CNC) by solution-casting method and then were covered with silver thin film by magnetron sputtering. The results showed that the surface modification increased the degree of crystallinity of nanocrystals from 51% to 56%, decreasing their length and diameter. Moreover, AFM-IR spectroscopy revealed that the modified CNCs were covered by adipic acid molecules, improving the dispersion of nanocrystals in PBAT. Well-dispersed modified CNCs acted as heterogeneous nuclei for crystallization of PBAT, and increased the storage modulus of the polymer by more than 200%. These improvements in thermal and mechanical properties of CNC-based PBAT associated with the decrease of 56% in the *Escherichia coli* biofilm formation on nanocomposites (antibacterial properties) qualify the CNC/PBAT nanocomposites covered with silver thin films to be used as food packaging. POLYM. ENG. SCI., 59:E356–E365, 2019. © 2019 Society of Plastics Engineers

INTRODUCTION

The use of biodegradable polymers as an alternative to nonbiodegradable ones offers a number of benefits for environmental conservation because of their nonharmful effects [1–6]. However, the mechanical properties of biodegradable polymers are usually poorer compared to many commonly used nonbiodegradable polymers, limiting their wide application [7]. The use of cellulose nanocrystals (CNCs) as reinforcement phase is a way to prepare biodegradable polymers with improved properties, maintaining the biodegradability of the matrix [8]. The critical challenges in the preparation of these nanocomposites come from the dispersion of CNCs in the surrounding matrix and interaction between filler/matrix, especially when low-polarity polymers are used [9, 10]. Surface modification of CNCs is an alternative to overcome this drawback, preventing the agglomeration and also improving interfacial interaction between CNC and polymer [11]. However, the mechanisms involved in the interaction between CNC and polymer are not fully clarified [12]. Several efforts have been made to prepare CNC-based nanocomposites with higher added value and to develop materials with prospective commercial application [13, 14]. In this context, the preparation of materials with antimicrobial activity has received great attention [15–18]. Here, we reported the preparation of poly(butylene adipate-co-terephthalate) (PBAT) filled with modified CNCs and covered with silver thin film. To our knowledge, the effects of CNC functionalization by adipic acid on the final properties of CNC/PBAT nanocomposites have not yet been reported. Moreover, this study has shown, for the first time, the use of magnetron sputtering for coating the CNC/PBAT nanocomposites with silver thin films. The increased mechanical strength of the nanocomposite combined with its antimicrobial property makes it a versatile material, which may be used as food packaging.

PBAT is a thermoplastic polyester usually synthesized by a polycondensation reaction between 1,4-butanediol, adipic acid, and terephthalic acid [19]. The linear random copolyester PBAT has attracted extensive attention from researchers because of its properties, such as flexibility [20], biodegradability [21], biocompatibility [22], Young's modulus of around 52 MPa [23], tensile strength of 32–36 MPa [24], and high elongation at break (700%) [25, 26]. These properties make PBAT be a viable candidate for several multifunctional applications, such as food packaging [27–30]. However, although PBAT has been recognized as a good material for a wide range of applications, it has failed to achieve the mechanical properties required in some applications, which limits its market [31]. In this context, research related to the development of nano-reinforced polymer composites has significantly increased to meet this need [32–35].

Cellulose is the most abundant polymer of the Earth, and several nano-sized materials can be obtained from it, such as cellulose nanofibrils (CNFs), bacterial nanocellulose, and CNCs [36,

Correspondence to: F.V. Ferreira; e-mail: filipevargasf@gmail.com

Contract grant sponsor: Conselho Nacional de Desenvolvimento Científico e Tecnológico. contract grant sponsor: Coordenação de Aperfeiçoamento de Pessoal de Nível Superior. contract grant sponsor: Fundação de Amparo à Pesquisa do Estado de São Paulo; contract grant number: 2016/09588-9.

DOI 10.1002/pen.25066

Published online in Wiley Online Library (wileyonlinelibrary.com).

37]. CNCs are nanomaterials widely used as reinforcing phase in polymer nanocomposites [38]. CNCs consist of rod-like particles measuring 5–50 nm in diameter and 100–1,000 nm in length, which can be obtained from various cellulose sources, such as *capim dourado* (*Syngonanthus nitens*) [39], ramie [40], and so on [41]. CNCs have outstanding physical properties, such as high aspect ratios, an estimated tensile strength of 0.3–22 GPa, elastic modulus of 105–168 GPa, and are commonly described as biocompatible and biodegradable [42, 43]. These properties are potentially useful for a wide range of applications, especially when the CNCs are used as reinforcement in polymer nanocomposites. Addition of CNCs in low-polarity polymers has been challenging because the inherent hydrophilicity of the CNCs leads to an inadequate dispersion and a weak interaction (poor wetting) with the matrix. Surface modification of the nanofiller is one of the most effective ways to overcome these drawbacks [44–46].

In general, CNC-based PBAT nanocomposites can be fabricated by two main methods: melt mixing and solvent casting [47–49]. It is well known that similar nanocomposites prepared by different methods can present very different properties [50]. Moreover, each method has advantages and disadvantages. Solvent casting seems to be a promising method to fabricate CNC-based PBAT because the CNCs can form a rigid H-bonded three-dimensional (3D) network inside the polymer [51]. The formation of this 3D network is only possible in casting method conditions because of the long time for reaction, which is enough for the particles to interact and self-organize [52]. CNC/PBAT nanocomposites with 3D particle network can show improved overall properties. To highlight the prospective application of the CNC/PBAT nanocomposites and increase their added value, a silver thin film can be added to the material. This thin film, formed by silver particles, presents antimicrobial activity and is well known for improving the antibacterial properties of polymeric materials [53, 54]. CNC/PBAT nanocomposites covered with silver thin film can be used, for example, to pack food.

Escherichia coli is one of the main pathogens involved in human diseases associated with food contamination [55]. For this reason, intervention measures used to ensure food safety by eliminating or inactivating this species from manufactured food products are needed [56]. These authors suggest that measures of control should target each stage of food chain. This study aimed to contribute to the packing stage of this chain.

In this study, we report the preparation of CNC/PBAT nanocomposites that present superior mechanical properties compared to the neat polymer and potential application as food packaging. The CNCs were isolated from sugarcane bagasse waste and functionalized by adipic acid. Nanocomposites were prepared with 0.5, 1, and 1.5 times the CNC content necessary to reach the theoretical percolation threshold and covered with silver thin film. Their thermal, mechanical, and antibacterial properties were studied and their prospective applications were discussed.

MATERIALS AND METHODS

Materials

Sugarcane bagasse was provided by Raízen (São Paulo, Brazil). Concentrated sulfuric acid (H_2SO_4, 95%–98%), ethanol (C_2H_6O, 95%), chloroform ($CHCl_3$), and adipic acid ($C_6H_{10}O_4$, 99%) were purchased from Aldrich. High-purity sodium hydroxide (NaOH) and a hydrogen peroxide (H_2O_2) solution were purchased from Syntharise Chemical. PBAT (Ecoflex®, M_n = 47,000 g/mol; M_w = 105,000 g/mol) was provided by BASF.

Isolation of CNCs

CNCs were isolated from sugarcane bagasse by acid hydrolysis as described elsewhere [57]. Briefly, bagasse pulp (10 g) was dispersed in 250 mL of sulfuric acid 65% at 45°C under mechanical stirring for 45 min to allow fiber hydrolysis. The hydrolyzed fibers were washed with deionized water (centrifugation, 4,500 rpm, 15 min per step) and dialyzed in deionized water for 3 days (until a neutral pH was reached). Then, the suspension was subjected to further centrifugation (6,500 rpm, 30 min) to separate nano-sized cellulose from micro-sized cellulose [58]. Finally, the CNC suspension was lyophilized. This sample was labeled CNC.

Surface Modification of CNCs

An amount of CNC (0.4 g) was dispersed into adipic acid solution (50 mL H_2O and 1 g adipic acid) and then four drops of H_2SO_4 were added. The suspension was kept at 80°C for 2 h with mechanical stirring. After that, the system was cooled to 40°C followed by successive centrifugation (14,000 rpm, 10 min per step) to remove free acid from the suspension. Finally, dialysis against distilled water was performed for 3 days (neutral pH) [57]. The modified CNC was labeled MCNC.

Preparation of CNC-Based Nanocomposites

Neat PBAT and CNC-based nanocomposites were prepared by solvent casting method. CNCs (functionalized and nonfunctionalized) were dispersed in chloroform (30 mL) using an ultrasonic bath during 30 min. After that, 5 g of PBAT was added into this premixed stage. The mixture was poured into a glass Petri dish and covered with a glass lid, leaving a gap of 0.25 mm between the dish and the lid. The Petri dishes were left in a fume hood during 24 h at room temperature for solvent evaporation. Nanocomposites were prepared with 0.5, 1, and 1.5 times the CNC content to reach the theoretical percolation threshold (i.e., 1.5 wt % CNC), which corresponds to 0.8, 1.5, and 2.3 wt% of CNCs. The theoretical percolation threshold was calculated based on dimensions of CNC determined by atomic force microscopy (AFM) according to Eq. 1:

$$\varphi_c = \frac{0.7}{(L/D)} \tag{1}$$

where Φ_c is the theoretical percolation threshold and L/D is the aspect ratio of CNC [59]. The density of the CNC and PBAT were 1.56 and 1.25 g cm^{-3}, respectively [60]. Nanocomposites with 0.8, 1.5, and 2.3 wt% of CNCs were labeled CNC1/PBAT, CNC2/PBAT, and CNC3/PBAT, respectively. Nanocomposites with 0.8, 1.5, and 2.3 wt% of MCNCs were labeled MCNC1/PBAT, MCNC2/PBAT, and MCNC3/PBAT, respectively.

Coating with Silver Thin Film by Magnetron Sputtering

The silver thin films were deposited onto pure PBAT and nanocomposites by magnetron sputtering technique with 20 sccm Ar flow and 3 mTorr working pressure, using 7 W DC power applied on a high-purity Ag target (99.99%) from Kurt J. Lesker

Company. The percentage of Ag inserted in the samples is related to the target sputter yield. Here, the parameters of the plasma process were kept constant for all samples. Thus, the formed thin film coating had the same amount of Ag. The schematic diagram of the deposition system is shown in Fig. 1. This thin film coating is able to enhance the surface properties of the material, while the bulk properties are not changed [61].

Characterization

X-Ray Photoelectron Spectroscopy (XPS). The surface modification of the CNCs was analyzed by XPS using a commercial spectrometer (Thermo Fisher Scientific, UK) equipped with Mg Kα line ($h\nu$ =1,253.6 eV) at low pressure and operated at 10 eV.

X-Ray Diffraction (XRD). The degree of crystallinity (I_c) of CNCs was studied using an X-ray diffraction (Philips X Pert X-ray diffractometer) with Cu-Kα (λ = 1.54060 Å), equipped with a diffractometer at 40 kV and current of 40 mA. The sample was scanned in a 2θ-angle range between 10° and 30° at room temperature. I_c was calculated based on the Segal method [62], according to Eq. 2:

$$I_c = \left[\frac{I_2 - I_1}{I_2}\right] \times 100 \quad (2)$$

where I_2 is the intensity associated with the crystalline peak (2θ = 22.9°) and I_1 is the intensity of the amorphous part (2θ = 18°).

Atomic Force Microscopy (AFM). AFM was performed in an NX10 atomic force microscope (Park System) operating on intermittent contact. The spring constant and resonant frequency of the silicon tip (nanosensors) were 42 N/m and 320 kHz, respectively. The samples were prepared as follows. A 10 μL drop of poly-L-lysine was deposited on freshly cleaned mica for 3 min, and then rinsed with deionized water and dried. A 10 μL drop of diluted CNC suspension (0.001 wt%) was placed on mica for 3 min and then rinsed with deionized water. The samples were dried under ambient conditions [63].

Atomic Force Microscopy-Based Infrared Spectroscopy (AFM-IR). AFM-IR measurements were performed on NanoIR2-s (Anasys Instruments, Santa Barbara, CA) at a repetition rate of 180 kHz from an infrared source (Quantum Cascade Lasers – Daylight) tuned to a wavelength corresponding to C=O absorption (at 1700 cm^{-1}). All AFM topographic images were obtained in contact mode with resonance frequency of 13 ± 4 kHz and a spring constant of 0.07–0.4 N/m [64]. The samples were prepared as follows. A 10 μL drop of diluted CNC suspension (0.001 wt%) was placed on a gold-coated substrate, and then the water was evaporated at room temperature.

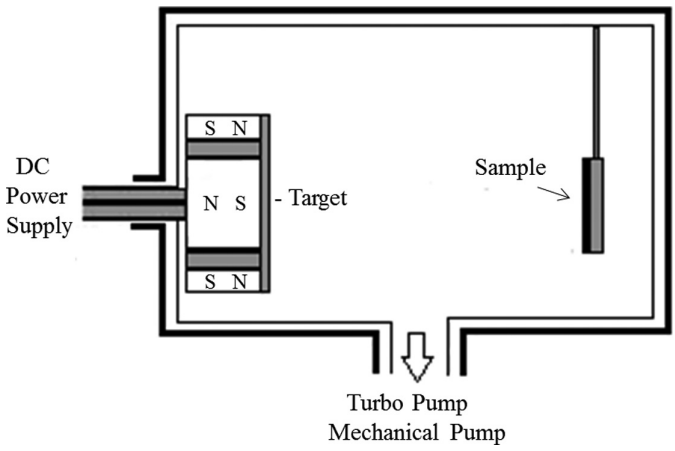

FIG. 1. Scheme of magnetron sputtering deposition system.

Differential Scanning Calorimetry (DSC). The thermal behavior of neat polymer and nanocomposites were evaluated using DSC 214 (TA Instruments, New Castle, DE). The samples (about 10 mg) were first heated to 180°C under a nitrogen atmosphere at a rate of 10°C/min to eliminate their thermal history. Then, the samples were cooled to −60°C followed by a second heating scan up to 180°C under nitrogen atmosphere at a rate of 10°C/min. The crystallinity (X_c) of neat polymer and nanocomposites was calculated using Eq. 3:

$$X_c = \frac{\Delta H_m}{\Delta H_m^\circ f_c} \times 100, \quad (3)$$

where ΔH_m is the enthalpy of the second melting peak (J/g), ΔH_m° (114 J/g) is the enthalpy of fusion for 100% pure crystalline PBAT, and f_c is the weight fraction of the polymer [47].

Dynamic Mechanical Analysis (DMA). DMA of neat PBAT and PBAT-based nanocomposites was performed using a Q800 DMA apparatus (TA Instruments, New Castle, DE) with a tensile film clamp in strain mode at 0.01 N controlled forces. The measurements were carried out at constant frequency (1 Hz), temperature range from −80°C to 80°C, and heating rate of 3°C/min. The sample specimen dimensions were around 16.5 × 6.5 × 0.6 mm. The modulus value was normalized to 3 MPa (at glassy state) to avoid possible experimental errors because of sample dimension measurements at room temperature, in which it is softer.

Antimicrobial Test. The effect of silver thin film coating on CNC/PBAT samples was evaluated on *E. coli* biofilm formation. We chose *E. coli* because of the potential application of CNC-based nanocomposites as food packaging. *E. coli* is used as an indicator of food and medical product contaminants [65, 66]. An *E. coli* ATCC 23922 standardized suspension containing 10^7 cells/mL was prepared in saline solution using a spectrophotometer. Then, the initial suspension was diluted 1:10 in brain heart infusion (BHI) broth for preparing the inoculum containing 10^6 cells/mL. The specimens (with 5 mm diameter and 0.2 mm thickness) were previously sterilized by UV radiation for 30 min. Aliquots of 20 μL of inoculum and 180 μL of BHI broth were transferred into a 96-well plate containing sterile neat PBAT and nanocomposites filled with MCNCs (MCNC1/PBAT, MCNC2/PBAT, and MCNC3/PBAT).

The samples were added to each well immersed in the culture medium and the plates were incubated at 37°C under agitation (90 rpm) for 120 min for preadherence phase, under aerobiosis. Later, the samples were washed with 1 mL of phosphate-buffered saline (PBS) and transferred to new wells with 200 μL of BHI broth and incubated for 24 h at 37°C under aerobiosis. Then, the samples were washed with 1 mL of PBS and transferred to tubes

containing 1 mL of saline solution. For biofilm disruption, tubes were vortexed for 30 s and then sonicated (3 pulses with 10 s interval, amplitude of 40 and 15 W). The initial suspensions were serially diluted in saline solution, obtaining dilutions from 10^{-1} to 10^{-4}, and plated on BHI agar. After incubation for 24 h at 37°C under aerobiosis, the number of colony forming units per specimen (CFU/specimen) was obtained and the variation in the number of colony forming units of the nanocomposites filled with modified CNCs was compared.

RESULTS AND DISCUSSION

X-Ray Photoelectron Spectroscopy

XPS analysis was used to investigate the chemical composition of CNCs before and after surface modification. High-resolution XPS spectra of C1s of CNC and MCNC (Fig. 2) showed four carbon peaks: C1 (~285 eV), associated with C—C/C—H bonds; C2 (~286 eV), associated with C–O of alcohols and ethers; C3 (~288 eV), associated with O—C—O; and C4 (~289 eV), associated with O—C═O (contribution of esters groups) [11]. Surface modification increased the magnitude of the C1 peak from 23.2% to 29.7% because of the long carbon chain of adipic acid. Simultaneously, the C4 peak increased (from 4.9% to 13.9%) and the C2 peak decreased (64.1% to 29.7%), probably because of the conversion of some of the alcohol and ether groups in the ester groups during the esterification reaction between the adipic acid and the CNCs [57]. Thus, the changes observed in the XPS spectra confirm the successful functionalization of CNCs.

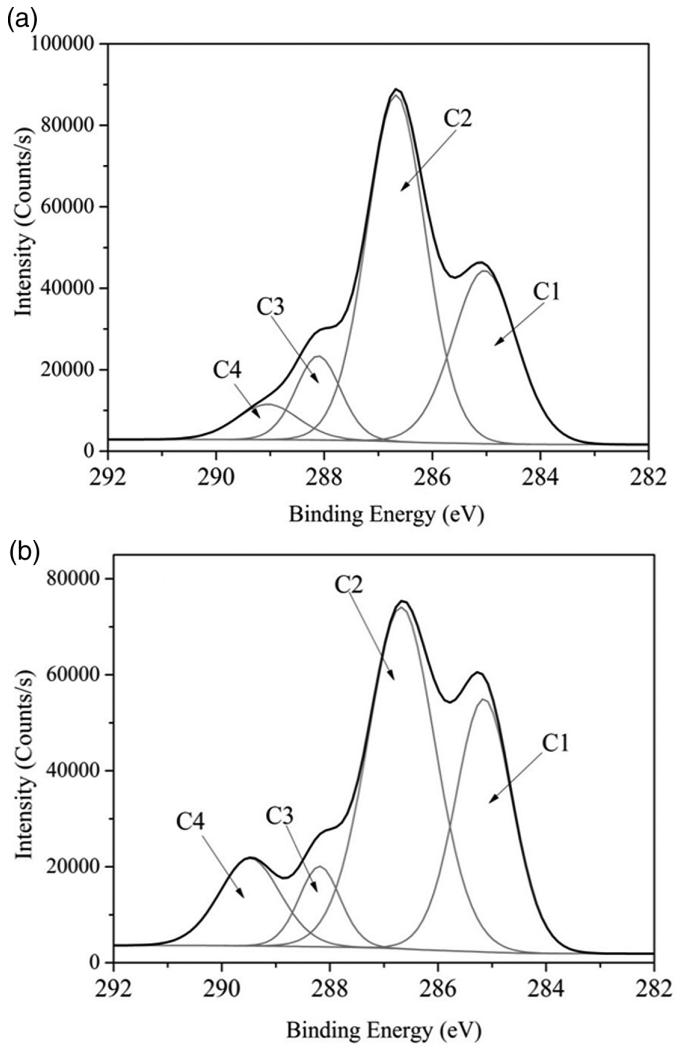

FIG. 2. Deconvoluted C1s XPS spectrum of (a) CNC and (b) MCNC.

X-Ray Diffraction Analysis

XRD experiments were performed to investigate the effect of functionalization on the degree of crystallinity (I_c) of CNCs. The XRD patterns of CNC and MCNC (Fig. 3) showed three diffraction peaks at 15.7° (1 0 1), 16.7° (0 1^{-}1), and 22.9° (0 0 2), corresponding to the crystalline structure of cellulose I, while the small peak at 20.6° (0 2 1) was related to amorphous regions [48]. We found that the I_c of the samples increased from 51% to 56% after functionalization, which could be related to a removal of some amorphous portion of cellulose after functionalization because of the faster hydrolysis of the amorphous portion compared to the hydrolysis of crystalline domains [67].

Atomic Force Microscopy

AFM was used to characterize the morphology and size distribution of CNCs before and after modification (Fig. 4). The length and diameter of CNCs were measured according to the method reported by Lahiji et al. [68]. CNCs had a rod-like characteristic aspect, with length of 362–463 nm and diameter of 8–12 nm, resulting in an aspect ratio of 41. After surface modification, the rod-like shape was preserved, but its length (185–300 nm) and diameter (5.1–8.5 nm) were decreased. As a result, the particle aspect ratio (35) was decreased. As XRD results showed that an amorphous part of CNCs was removed after surface modification (increasing the degree of crystallinity of the sample), the decrease of length and diameter of CNCs after surface modification can be related to the removal of the amorphous region between the crystalline domains (or even at their extremities) during the functionalization, resulting in nanocrystals with smaller dimensions. This

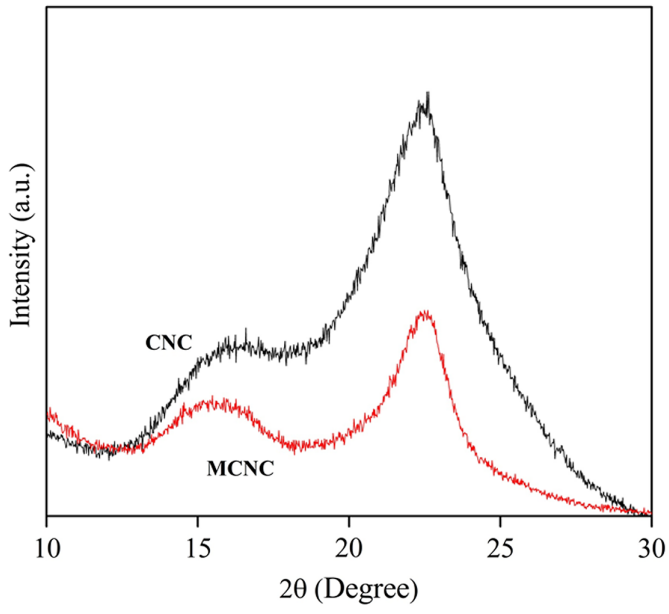

FIG. 3. XRD diffractograms of (a) CNC and (b) MCNC.

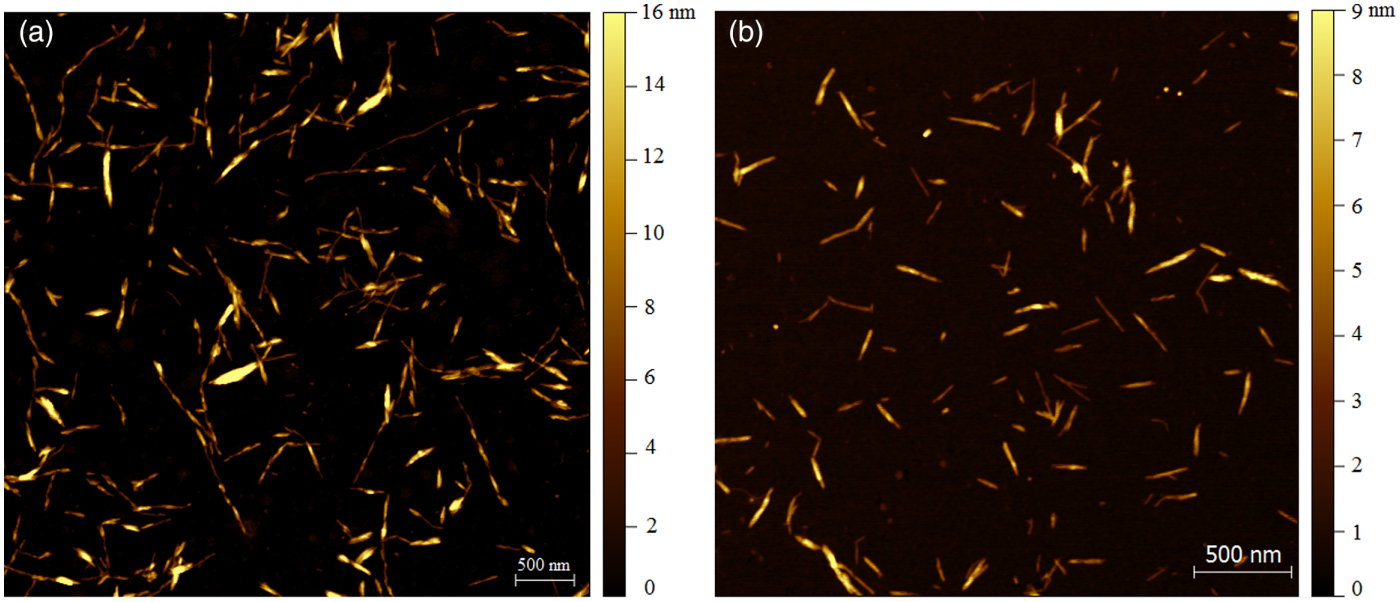

FIG. 4. AFM images of (a) CNC and (b) MCNC.

issue was best discussed in our recent article [57] and was also reported by other authors [69]. The dimensions of CNCs isolated from the sugarcane bagasse are close to the dimensions of CNCs reported by other authors [70, 71].

Dispersion Study

The dispersion behavior of CNCs in chloroform and PBAT matrix was investigated based on the visual aspect of the systems. Moreover, an additional understanding of how the functional group attached to the CNC interacts with the medium was qualitatively discussed based on AFM along with IR technique (AFM-IR). AFM-IR spectroscopy combines the spatial resolution of AFM with the chemical analysis capability of IR spectroscopy [72]. During the analysis, an IR source is tuned at a specific wavelength (in our case at 1,700 cm^{-1}; C═O absorption) [73, 74]. The sample with group C═O in abundance vibrates and the thermal expansion in response to infrared excitation is detected [75]. The blue region in the chemical images obtained at 1,700 cm^{-1} indicates low infrared absorptivity, while the orange region indicates areas of greater absorptivity, that is, a greater amount of group C═O. Thus, this technique is a powerful tool to identify the functional groups chemically attached on CNC and can help to clarify the mechanisms involved in the interaction between CNC and PBAT.

The results showed that the unmodified CNCs remained in clusters in the chloroform (Fig. 5a). A same pattern of agglomerated particles can be observed in the PBAT (red circle in Fig. 5b), reflecting its poor dispersion in organic solvent and low-polarity polymer. On the other hand, modified CNCs showed good dispersion in chloroform at same time that no visible agglomeration in PBAT was observed. The good dispersion of MCNCs in chloroform and PBAT can be related to the adipic acid attached to the MCNCs surface. This was confirmed by AFM-IR (Fig. 5c), which showed that modified CNCs are covered by adipic acid molecules with the characteristic IR vibrational spectra peak at 1,698 cm^{-1} (Fig. 5d), associated with its C═O stretching vibrations ν(C═O). A hypothetical explanation of good interaction of modified CNCs with chloroform and PBAT can be related to the core–shell structure of modified CNC (Fig. 5e). In this context, the long adipic acid chains bound to the MCNC surface decrease the inherent hydrophilicity of CNCs, improving their interaction with organic solvent and low-polarity polymer. A similar behavior was observed by Kaboorani and Riedl [76]. The authors showed that functional groups attached in the CNCs surface can improve the CNC dispersibility in organic solvents.

Differential Scanning Calorimetry

DSC was performed to assess the effect of CNCs on the crystallization of the PBAT matrix (Fig. 6). The melting temperature peak was 129°C for all samples. The results of the enthalpy of fusion (ΔH_m), crystallization temperature (T_c), and crystallinity (X_c) are summarized in Table 1. We observed that the ΔH_m of the PBAT increased after addition of 0.8 and 1.5 wt% of unmodified CNCs (CNC1/PBAT and CNC2/PBAT, respectively), corroborating previous results found in the literature for similar unmodified CNC concentrations [52]. Such addition resulted in materials with higher crystallinity in all studied compositions. On the other hand, ΔH_m decreased along with X_c for nanocomposites reinforced with modified CNCs (MCNC/PBAT samples). This suggests that crystals formed from MCNC nanoparticles are able to present a well-defined structure, with a sharp range of temperatures during melting compared to neat polymer or CNC/PBAT nanocomposite. No significant change in T_c was observed after addition of unmodified CNC, while T_c shifted to a slightly higher temperature as the content of the MCNC increased. A more pronounced effect was observed for the nanocomposites reinforced with 1.5 wt% modified CNCs. This increase in T_c is probably related to improved dispersion of the nanofiller into the polymer matrix [77, 78]. Well-dispersed CNCs can lead to an increased number of heterogeneous nuclei for crystallization (nucleation sites) [79, 80]. The increase in number of heterogeneous nuclei for crystallization is directly related to an increased T_c [81, 82].

 DOI 10.1002/pen

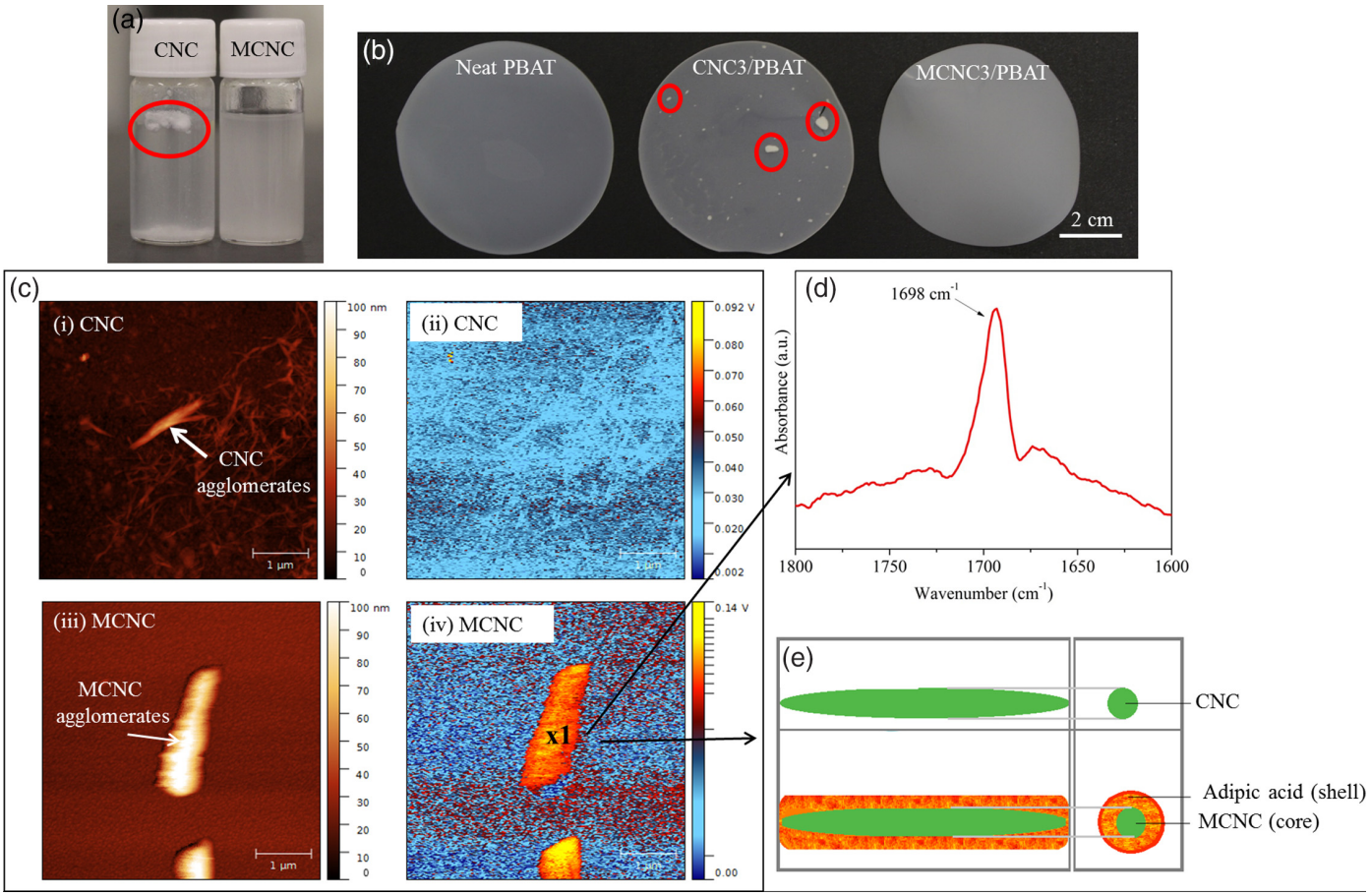

FIG. 5. (a) Images of CNC and MCNC in chloroform (0.3 mg/mL) after sonication for 30 min. (b) Neat polymer and nanocomposites prepared with 0.8 wt% cellulose nanocrystals. (c) (i and iii) Height mode AFM images and (ii and iv) chemical images obtained at 1,700 cm^{-1} for the CNC and MCNC samples. (d) IR vibrational spectra of point 1 from AFM images of MCNC. (e) A model of the CNC coated with adipic acid.

Dynamic Mechanical Analysis

Figure 7a and b shows the evolution of the logarithm of the storage modulus (E') and loss modulus (E'') measured at a frequency of 1 Hz as a function of temperature. The values of E' and glass transition temperature (T_g) are summarized in Table 2. Three distinct glassy–viscoelastic–rubbery regions can be observed in Fig. 7a, which are characteristics of thermoplastic materials. At the glassy region (first plateau), no significant changes between

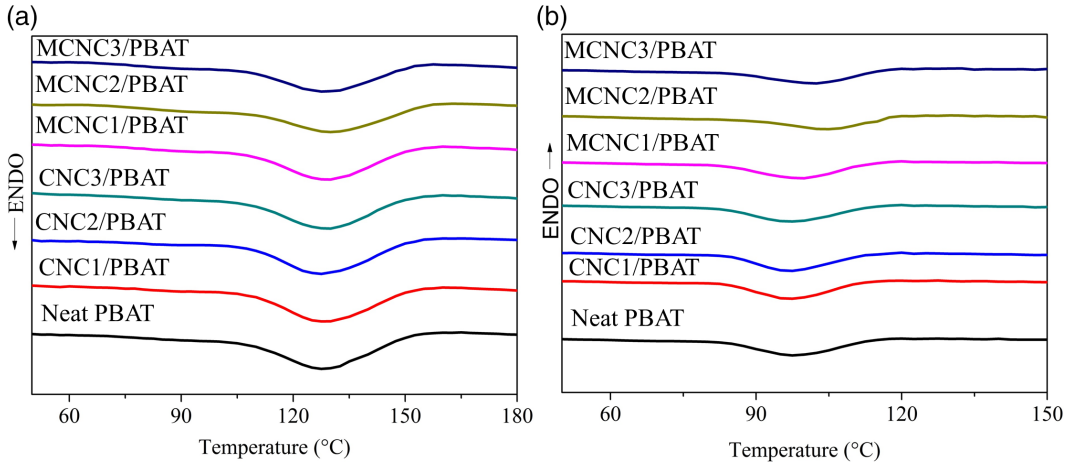

FIG. 6. DSC curves of neat PBAT and nanocomposites. (a) Second heating and (b) cooling under nitrogen atmosphere.

TABLE 1. - Values of ΔH_m, T_c, and X_c of neat PBAT and PBAT-based nanocomposites.

Sample	ΔH_m (J/g)	T_c (°C)	X_c (%)
Neat PBAT	10.5	97.6	9.2
CNC1/PBAT	10.7	97.0	9.4
CNC2/PBAT	11.6	97.4	10.4
CNC3/PBAT	10.4	97.8	9.4
MCNC1/PBAT	10.4	99.5	9.1
MCNC2/PBAT	8.7	105.0	7.8
MCNC3/PBAT	8.7	102.0	7.9

TABLE 2. - Variation of E' and T_g of PBAT and nanocomposites. E'/E'_{PBAT} indicates the increase of the value of the nanocomposites when compared with neat PBAT.

Samples	E' at 75°C (MPa)	E'/E'_{PBAT}	T_g (°C)[aa]
Neat PBAT	475	1.0	−31
CNC1/PBAT	700	1.5	−30
CNC2/PBAT	860	1.8	−30
CNC3/PBAT	924	2.0	−27
MCNC1/PBAT	993	2.1	−29
MCNC2/PBAT	1,102	2.3	−27
MCNC3/PBAT	1,324	2.8	−29

[a]T_g obtained by the curves of the loss modulus.

the storage modulus of the samples can be observed. This behavior occurs because, at low temperatures (below −40°C), the polymer stiffness hides the mechanical effect caused by the presence of a CNC network and polymer/filler interactions. On the other hand, a modulus decrease is observed in temperatures higher than −30°C. This transition region is associated with the softening of the polymer chains because of the temperature increase, being related to the polymer T_g [83]. Figure 7b and Table 2 show that the addition of CNC (especially above theoretical percolation threshold) changed the T_g of the nanocomposites, meaning that CNCs are affecting the relaxation of the PBAT amorphous phase. At higher temperatures (above −14°C), the rubbery region (second plateau) of the PBAT was strongly affected by the addition of CNCs. The storage modulus enhanced as the unmodified CNC content increased. This increase in E' can be related to the presence of fillers, which are able to act as reinforcement agent by causing filler/polymer entanglements or by increasing the crystallinity of the nanocomposites compared to the neat polymer. Morelli et al. [84] prepared PBAT-based nanocomposites reinforced with CNC and reported that the increase in the elastic modulus is related to the increase in rigidity of the material because of higher crystallinity. However, the nanocomposites prepared here with modified CNCs showed lower crystallinity (as discussed by DSC analysis, Table 1). In this case, the filler reinforcement seems to arise as a result of polymer chain immobilization. As suggested by Mariano et al. [49], the addition of a certain volume fraction of CNCs (percolation threshold) in the PBAT by casting method can generate interconnected structures; that is, a rigid 3D particle network that is based on hydrogen bonding between the nanoparticles, which affect the rubbery state of the matrix. As the content of CNCs increases, such interactions begin to dominate, resulting in the formation of a CNC–polymer network [85, 86]. The reinforcement effect on these auto-reorganized structures is more pronounced when the CNC–matrix interactions are improved. Thus, the higher values of elastic modulus observed for nanocomposites prepared with MCNCs, when compared to their counterparts prepared with CNC, seem to have this origin. These results allow us to conclude that the surface modification of CNCs improves fillers interaction with PBAT. Moreover, the reinforcing effect of CNCs is probably governed by both contributions from crystallinity and the interaction between the surface of the nanofiller and the PBAT.

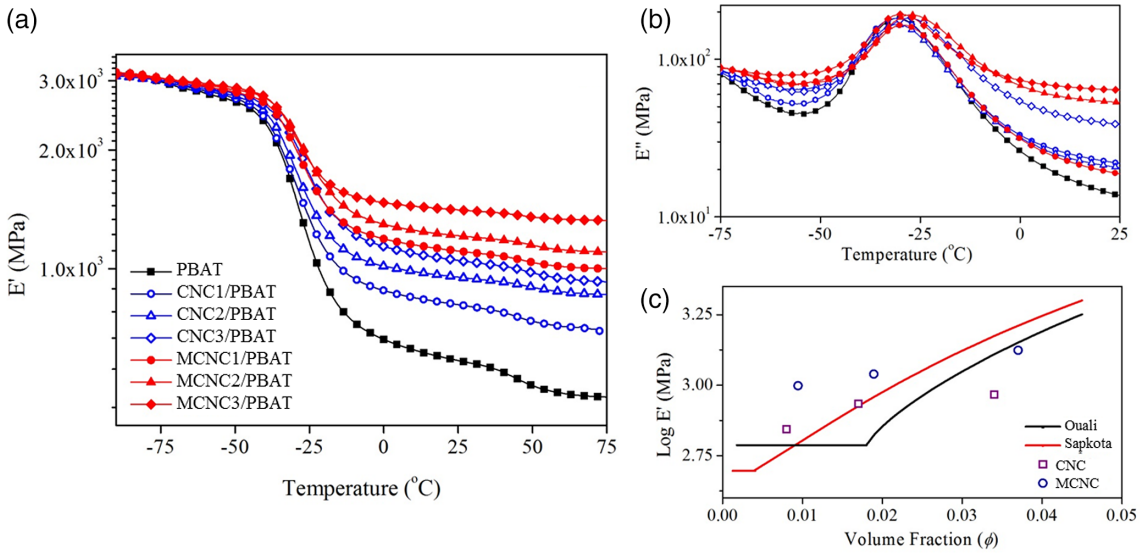

FIG. 7. Evolution of the logarithm of the (a) storage modulus (E') and (b) loss modulus (E'') of the neat PBAT and the nanocomposites loaded with cellulose nanocrystals as a function of temperature (at a frequency of 1 Hz). (c) Experimental data (at 75°C) and theoretical models: (□) CNC/PBAT, (○) MCNC/PBAT; red line corresponds to the Ouali–Takayanagi model and black line corresponds to the Sapkota et al. [76] model.

DOI 10.1002/pen

Some theoretical models can be used to predict mechanical properties of nanocomposites. In the presence of the percolated network, the model developed by Ouali–Takayanagi is precise to describe the E' behavior above the percolation threshold. This model is shown by Eqs. 4 and 5 [87, 88].

$$E' = \frac{(1-2\emptyset+\emptyset Xr)EsEr+(1-Xr)\emptyset Er2}{(1-Xr)Er+(Xr-\emptyset)Es} \quad (4)$$

$$\begin{cases} 0 \; if \; Xr < \psi c \\ Xr\left(\frac{Xr-\psi c}{1-\psi c}\right)^{0.4} \; if \; Xr > \psi c \end{cases} \quad (5)$$

$$\Psi c \, \frac{0.7}{L/d} \quad (6)$$

where X_r is the volume fraction of the CNC on the nanocomposite; Ψc is the percolation threshold of the nanocomposite, normally defined by Eq. 6; E_r and E_s are the pristine modulus of rigid particles and matrix (assumed as 120 GPa for the filler and 475 MPa for the polymer); and $\emptyset$ is the volume fraction of particles that actually contributes to the formation of the network [87, 88].

Figure 7c shows the experimental data (at 75°C) and theoretical models. There was a weak relation between experimental and theoretical (Ouali–Takayanagi model) results. In fact, the model is not accurate to describe the E' for volume fractions smaller than the percolation volume ($X_r < \psi_c$ or $\emptyset = 0.02$). Above this value, the volume seems to be well-adjusted for the MCNC sample, but it predicts higher values than those found for the CNC sample. This can be explained by the presence of aggregates in the CNC sample, as discussed above. To obtain a model able to predict the E' below the percolation volume, Sapkota et al. [89] present a model that considers the overlapping of particles during the creation of the percolated network (α). This model allows the calculation of an alternative percolation threshold, shown by Eqs. 7 and 8, which can be used in Eqs. 4 and 5 to predict the mechanical properties of the nanocomposites. The model proposed by Sapkota et al. shows a good agreement with experimental data of the CNC-based PBAT nanocomposite at lower volume fractions of particles. However, the model is also not accurate to predict the E' values for MCNC-based PBAT nanocomposites (Fig. 7c). This behavior can be related to the high interaction of MCNC with the PBAT because of the surface modification. Such strong attraction cannot be predicted by the model. Here, the adjustment of the experimental data for the model (CNC-based nanocomposite) provides an α value around 2.

$$\psi c = \frac{2(1+\xi)-2\left(1+\frac{\xi}{2}\right)^{\frac{1}{2}}}{3\left(1+\frac{2}{3}\xi\right)} \quad (7)$$

$$\xi(\alpha,\gamma) = \frac{\left(1+\frac{2}{3\gamma}\right)\frac{1}{\gamma}}{\frac{8}{3\gamma^2}((1+\alpha)|3-1)+\frac{4}{\gamma}((1+\alpha)2-1)+\alpha} \quad (8)$$

γ is the sample aspect ratio (L/d).
α is the connectivity variable ($\alpha = \lambda/D - 1$).

Antimicrobial Test

The nanocomposites with the best mechanical properties (MCNC1/PBAT, MCNC2/PBAT, and MCNC3/PBAT) were covered with silver thin film by magnetron sputtering technique to highlight the potential of these nanocomposites for different applications. The results showed that the content of MCNC affects the bacteria growth on the nanocomposites, avoiding biofilm formation. The greatest antimicrobial effect was observed for the nanocomposite filled with 0.8 wt% MCNC, with a decrease of 56% when compared to neat PBAT. This effect decreased as the MCNC content increased, with a decrease of 32% for the nanocomposite filled with 1.5 wt% MCNC and an increase of 30% for the composite filled with 2.3 wt% MCNC. These results suggest an interaction of the bacteria with the MCNCs. Probably, a smaller amount of MCNCs leads to a well-dispersed nanofiller, resulting in a worse condition for microorganism proliferation, which decreases the bacterial viability. When the amount of MCNC increases, some nanofillers can agglomerate, decreasing the efficient antimicrobial properties of the nanocomposites. These results are in agreement with previous studies, showing that the filler can affect the antimicrobial effect of the nanocomposites. Mondal et al. [90] showed that PBAT-based nanocomposites filled with modified montmorillonite present different antimicrobial effects according to the content of natural filler. *E. coli* was selected in this investigation due to the need of new methods to inactivate or eliminate this species from manufactured food products [56]. However, future evaluation of other microbial species would be interesting to detect new applications of the proposed material.

CONCLUSIONS

By AFM-IR spectroscopy, we have shown that the surface group attached on CNC forms a core–shell structure that affects the interaction of the CNC surface with the polymer. The nanocomposites filled with modified CNCs present better dispersion and greater interaction with PBAT, resulting in nanocomposites with improved mechanical properties. This improvement is more pronounced as the CNC content increases. The nanocomposites covered with silver thin film by magnetron sputtering show antimicrobial activity against *E. coli*, which depends on the MCNC content. The results reported in this study support the idea that the increased mechanical strength of the nanocomposites filled with 0.8 wt% MCNC combined with their antimicrobial property make them a versatile material, which has the potential to be used in food packaging.

ACKNOWLEDGMENTS

The authors thank São Paulo Research Foundation – FAPESP (PhD fellowship of F.V.F), CAPES and CNPq, and LNNano/CNPEM for the support received in AFM, AFM-IR, and XPS analyses. The authors also thank the Espaço da Escrita – Pró-Reitoria de Pesquisa – UNICAMP for the language services provided.

REFERENCES

1. R. Geyer, J.R. Jambeck, and K.L. Law, *Sci. Adv.*, **3**, e1700782 (2017).
2. R.A. Gross, *Science*, **297**, 803 (2002).
3. F. Sarasini, J. Tirillò, A. Zuorro, G. Maffei, R. Lavecchia, D. Puglia, F. Dominici, F. Luzi, T. Valente, and L. Torre, *Ind. Crop. Prod.*, **118**, 311 (2018).

4. N. Pantoustier, B. Lepoittevin, M. Alexandre, P. Dubois, D. Kubies, C. Calberg, and R. Jérôme, *Polym. Eng. Sci.*, **42**, 1928 (2002).
5. T.-M. Wu and M.-F. Chiang, *Polym. Eng. Sci.*, **45**, 1615 (2005).
6. R.P. Rosa, F.V. Ferreira, A.P.K. Saravia, S.A. Rocco, M. L. Sforça, R.F. Gouveia, and L.M.F. Lona, *Ind. Eng. Chem. Res.*, **57**, 13387 (2018).
7. M.K. Thakur, V.K. Thakur, R.K. Gupta, and A. Pappu, *ACS Sustain. Chem. Eng.*, **4**, 1 (2016).
8. H. Kargarzadeh, M. Mariano, J. Huang, N. Lin, I. Ahmad, A. Dufresne, and S. Thomas, *Polymer (Guildf)*, **132**, 368 (2017). https://doi.org/10.1016/j.polymer.2017.09.043.
9. K. Oksman, Y. Aitomäki, A.P. Mathew, G. Siqueira, Q. Zhou, S. Butylina, S. Tanpichai, X. Zhou, and S. Hooshmand, *Compos. A: Appl. Sci. Manuf.*, **83**, 2 (2016).
10. A. Vatansever, H. Dogan, T. Inan, S. Sezer, and A. Sirkecioglu, *Polym. Eng. Sci.*, **55**, 2922 (2015).
11. F.V. Ferreira, I.F. Pinheiro, R.F. Gouveia, G.P. Thim, and L.M. F. Lona, *Polym. Compos.*, **39**, E9 (2018).
12. F.V. Ferreira, A. Dufresne, I.F. Pinheiro, D.H.S. Souza, R. F. Gouveia, L.H.I. Mei, and L.M.F. Lona, *Eur. Polym. J.*, **108**, 274 (2018).
13. H.M.C. Azeredo, M.F. Rosa, and L.H.C. Mattoso, *Ind. Crop. Prod.*, **97**, 664 (2017).
14. A. Dufresne, *Curr. Opin. Colloid Interface Sci.*, **29**, 1 (2017).
15. D. Wei, H. Wang, Z. Ziaee, F. Chibante, A. Zheg, and H. Xiao, *Mater. Sci. Eng. C*, **58**, 986 (2016).
16. C.L. Morelli, M. Mahrous, M.N. Belgacem, M.C. Branciforti, R. E.S. Bretas, and J. Bras, *Ind. Crop. Prod.*, **70**, 134 (2015).
17. R. Chang, D. Rohindra, R. Lata, K. Kuboyama, and T. Ougizawa, *Polym. Eng. Sci.* (2018). https://doi.org/10.1002/pen.24950.
18. P. Persico, V. Ambrogi, C. Carfagna, P. Cerruti, I. Ferrocino, and G. Mauriello, *Polym. Eng. Sci.*, **49**, 1447 (2009).
19. F.V. Ferreira, L.S. Cividanes, R.F. Gouveia, and L.M.F. Lona, *Polym. Eng. Sci.* (2018). https://doi.org/10.1002/pen.24770.
20. L. Jiang, M.P. Wolcott, and J. Zhang, *Biomacromolecules*, **7**, 199 (2006).
21. I.F. Pinheiro, F.V. Ferreira, D.H.S. Souza, R.F. Gouveia, L.M. F. Lona, A.R. Morales, and L.H.I. Mei, *Eur. Polym. J.*, **97**, 356 (2017).
22. G.F. Santana-Melo, B.V.M. Rodrigues, E. da Silva, R. Ricci, F. R. Marciano, T.J. Webster, L.M.R. Vasconcellos, and A. O. Lobo, *Colloids Surf. B: Biointerfaces*, **155**, 544 (2017).
23. P. Bordes, E. Pollet, and L. Averous, *Prog. Polym. Sci.*, **34**, 125 (2009).
24. V. Nagarajan, M. Misra, and A.K. Mohanty, *Ind. Crop. Prod.*, **42**, 461 (2013).
25. J.M. Raquez, Y. Nabar, R. Narayan, and P. Dubois, *Macromol. Mater. Eng.*, **293**, 310 (2008).
26. M. Shahlari and S. Lee, *Polym. Eng. Sci.*, **52**, 1420 (2012).
27. J.S. Pereira da Silva, J.M. Farias da Silva, B.G. Soares, and S. Livi, *Compos. Part B*, **129**, 117 (2017).
28. W.A. Ribeiro Neto, A.C.C. de Paula, T.M.M. Martins, A. M. Goes, L. Averous, G. Schlatter, and R.E. Suman Bretas, *Polym. Degrad. Stab.*, **120**, 61 (2015).
29. J.G. de Castro, B.V.M. Rodrigues, R. Ricci, M.M. Costa, A.F. C. Ribeiro, F.R. Marciano, and A.O. Lobo, *RSC Adv.*, **6**, 32615 (2016).
30. H. Moustafa, C. Guizani, C. Dupont, V. Martin, M. Jeguirim, and A. Dufresne, *ACS Sustain. Chem. Eng.*, **5**, 1906 (2017).
31. K. Fukushima, M.H. Wu, S. Bocchini, A. Rasyida, and M. C. Yang, *Mater. Sci. Eng. C*, **32**, 1331 (2012).
32. F.V. Ferreira, B.R.C. Menezes, W. Franceschi, E.V. Ferreira, K. Lozano, L.S. Cividanes, A.R. Coutinho, and G.P. Thim, *Fuller. Nanotubes Carbon Nanostruct.*, **25**, 25 (2017). https://doi.org/10.1080/1536383X.2017.1359553.
33. R. Scaffaro and A. Maio, *Chem. Eng. J.*, **308**, 1034 (2017).
34. B.R.C. de Menezes, F.V. Ferreira, B.C. Silva, E.A.N. Simonetti, T.M. Bastos, L.S. Cividanes, and G.P. Thim, *J. Mater. Sci.*, **53**, 14311 (2018).
35. L.S. Cividanes, W. Franceschi, F.V. Ferreira, B.R.C. Menezes, R.C.M. Sales, and G.P. Thim, *Mater. Res. Express*, **4**, 105101 (2017).
36. R.J. Moon, A. Martini, J. Nairn, J. Simonsen, and J. Youngblood, *Chem. Soc. Rev.*, **40**, 3941 (2011).
37. Y.-H. Feng, T.-Y. Cheng, W.-G. Yang, P.-T. Ma, H.-Z. He, X.-C. Yin, and X.-X. Yu, *Ind. Crop. Prod.*, **111**, 285 (2018).
38. R. Scaffaro, L. Botta, F. Lopresti, A. Maio, and F. Sutera, *Cellulose*, **24**, 447 (2017).
39. G. Siqueira, H. Abdillahi, J. Bras, and A. Dufresne, *Cellulose*, **17**, 289 (2010).
40. A. Junior de Menezes, G. Siqueira, A.A.S. Curvelo, and A. Dufresne, *Polymer (Guildf)*, **50**, 4552 (2009).
41. Y. Habibi, L.A. Lucia, and O.J. Rojas, *Chem. Rev.*, **110**, 3479 (2010).
42. A. Šturcova, I. His, D.C. Apperley, J. Sugiyama, and M.C. Jarvis, *Biomacromolecules*, **5**, 1333 (2004).
43. E. Espino-Pérez, S. Domenek, N. Belgacem, C. Sillard, and J. Bras, *Biomacromolecules*, **15**, 4551 (2014).
44. W. Francisco, F.V. Ferreira, E.V. Ferreira, L.D.S. Cividanes, A. d.R. Coutinho, and G.P. Thim, *J. Aerosp. Technol. Manag.*, **7**, 289 (2015).
45. J. Tang, J. Sisler, N. Grishkewich, and K.C. Tam, *J. Colloid Interface Sci.*, **494**, 397 (2017).
46. F. V. Ferreira, L. D. S. Cividanes, F. S. Brito, B. R. C. de Menezes, W. Franceschi, E. A. N. Simonetti, G. P. Thim, Functionalization of Carbon Nanotube and Applications, in: 2016: pp. 31–61. https://doi.org/10.1007/978-3-319-35110-0_2.
47. C.L. Morelli, M.N. Belgacem, M.C. Branciforti, R.E.S. Bretas, A. Crisci, and J. Bras, *Compos. A: Appl. Sci. Manuf.*, **83**, 80 (2016).
48. C.L. Morelli, M.N. Belgacem, M.C. Branciforti, M. C. B. Salon, J. Bras, and R.E.S. Bretas, *Polym. Eng. Sci.*, **56**, 1339 (2016).
49. M. Mariano, N. El Kissi, and A. Dufresne, *Langmuir*, **32**, 10093 (2016).
50. F. Alloin, A. D'Aprea, A. Dufresne, N. El Kissi, and F. Bossard, *Cellulose*, **18**, 957 (2011).
51. V. Favier, G.R. Canova, J.Y. Cavaillé, H. Chanzy, A. Dufresne, and C. Gauthier, *Polym. Adv. Technol.*, **6**, 351 (1995).
52. M. Mariano, C. Chirat, N. El Kissi, and A. Dufresne, *J. Polym. Sci. Part B: Polym. Phys.*, **54**, 2284 (2016).
53. H.-Y. Yu, X.-Y. Yang, F.-F. Lu, G.-Y. Chen, and J.-M. Yao, *Carbohydr. Polym.*, **140**, 209 (2016).
54. E. Fortunati, M. Peltzer, I. Armentano, A. Jiménez, and J. M. Kenny, *J. Food Eng.*, **118**, 117 (2013).
55. S. Galié, C. García-Gutiérrez, E.M. Miguélez, C.J. Villar, and F. Lombó, *Front. Microbiol.*, **9**, 898 (2018). https://doi.org/10.3389/fmicb.2018.00898.

56. N. H. Kim, T. J. Cho, M. S. Rhee, 2017, pp. 1–47.
57. F.V. Ferreira, M. Mariano, S.C. Rabelo, R.F. Gouveia, and L.M. F. Lona, *Appl. Surf. Sci.*, **436**, 1113 (2018).
58. W. Bai, J. Holbery, and K. Li, *Cellulose*, **16**, 455 (2009).
59. G. Siqueira, J. Bras, and A. Dufresne, *Polymers (Basel)*, **2**, 728 (2010).
60. A. Dufresne, *Nanocellulose: From Nature to High Performance Tailored Materials*, Walter De Gruyter, Berlin (2013).
61. M. Aliofkhazraei, *Nanocoatings*, Springer Berlin Heidelberg, Berlin, Heidelberg, Berlin (2011).
62. L. Segal, J.J. Creely, A.E. Martin, and C.M. Conrad, *Text. Res. J.*, **29**, 786 (1959).
63. M. Salajkova, L.a. Berglund, Q. Zhou, M. Salajková, L. a. Berglund, and Q. Zhou, *J. Mater. Chem.*, **22**, 19798 (2012).
64. F.V. Ferreira, F.S. Brito, W. Franceschi, E.A.N. Simonetti, L. S. Cividanes, M. Chipara, and K. Lozano, *Surf. Interfaces*, **10**, 100 (2018).
65. J.M. Rangel, P.H. Sparling, C. Crowe, P.M. Griffin, and D. L. Swerdlow, *Emerg. Infect. Dis.*, **11**, 603 (2005).
66. M.G. Rowland, R.A. Barrell, and R. Whitehead, *Lancet*, **311**, 136 (1978).
67. E. Ramires and A. Dufresne, *TAPPI J.*, **10**, 16 (2011).
68. R.R. Lahiji, X. Xu, R. Reifenberger, A. Raman, A. Rudie, and R. J. Moon, *Langmuir*, **26**, 4480 (2010).
69. W. Shang, J. Huang, H. Luo, P.R. Chang, J. Feng, and G. Xie, *Cellulose*, **20**, 179 (2013).
70. C. Liu, B. Li, H. Du, D. Lv, Y. Zhang, G. Yu, X. Mu, and H. Peng, *Carbohydr. Polym.*, **151**, 716 (2016).
71. G. Siqueira, J. Bras, and A. Dufresne, *Biomacromolecules*, **10**, 425 (2009).
72. A. Dazzi, C.B. Prater, Q. Hu, D.B. Chase, J.F. Rabolt, and C. Marcott, *Appl. Spectrosc.*, **66**, 1365 (2012).
73. F.V. Ferreira, W. Franceschi, B.R.C. Menezes, A.F. Biagioni, A. R. Coutinho, and L.S. Cividanes, *Carbon-Based Nanofillers and their Rubber Nanocomposites*, Elsevier, Amsterdam, Netherlands, 1 (2019).
74. F.V. Ferreira, W. Francisco, B.R.C. De Menezes, L.D. S. Cividanes, A.D.R. Coutinho, and G.P. Thim, *Appl. Surf. Sci.*, **357**, 2154 (2015). https://doi.org/10.1016/j.apsusc.2015.09.202.
75. A. Dazzi, C. B. Prater, *Chem. Rev.*, **117**, 5173 (2017).
76. A. Kaboorani and B. Riedl, *Ind. Crop. Prod.*, **65**, 45 (2015).
77. R. Botan, I.F. Pinheiro, F.V. Ferreira, and L.M.F. Lona, *Mater. Res. Express*, **5**, 65004 (2018).
78. F.V. Ferreira, L.D.S. Cividanes, F.S. Brito, B.R.C. de Menezes, W. Franceschi, E.A. Nunes Simonetti, and G.P. Thim, *Functionalizing Graphene and Carbon Nanotubes: A Review*, Springer International Publishing, Cham (2016).
79. F.V. Ferreira, W. Franceschi, B.R.C. Menezes, F.S. Brito, K. Lozano, A.R. Coutinho, L.S. Cividanes, and G.P. Thim, *Appl. Surf. Sci.*, **410**, 267 (2017).
80. F. V. Ferreira, L. D. S. Cividanes, F. S. Brito, B. R. C. de Menezes, W. Franceschi, E. A. N. Simonetti, G. P. Thim, Functionalization of Graphene and Applications, in: 2016: pp. 1–29. https://doi.org/10.1007/978-3-319-35110-0_1
81. M.A.L. Manchado, L. Valentini, J. Biagiotti, and J.M. Kenny, *Carbon N. Y.*, **43**, 1499 (2005).
82. F.V. Ferreira, W. Francisco, B.R.C. Menezes, F.S. Brito, A. S. Coutinho, L.S. Cividanes, A.R. Coutinho, and G.P. Thim, *Appl. Surf. Sci.*, **389**, 921 (2016).
83. M. Mariano, N. El Kissi, and A. Dufresne, *Eur. Polym. J.*, **69**, 208 (2015).
84. C.L. Morelli, N. Belgacem, R.E.S. Bretas, and J. Bras, *J. Appl. Polym. Sci.*, **133**, 1 (2016).
85. J. Sapkota, S. Kumar, C. Weder, and E.J. Foster, *Macromol. Mater. Eng.*, **300**, 562 (2015).
86. P. Dhar, D. Tarafder, A. Kumar, and V. Katiyar, *RSC Adv.*, **5**, 60426 (2015).
87. L. Tang and C. Weder, *ACS Appl. Mater. Interfaces*, **2**, 1073 (2010).
88. J.R. Capadona, O. Van Den Berg, L.a. Capadona, M. Schroeter, S. J. Rowan, D.J. Tyler, and C. Weder, *Nat. Nanotechnol.*, **2**, 765 (2007).
89. J. Sapkota, J.C. Martinez Garcia, and M. Lattuada, *J. Appl. Polym. Sci.*, **134**, 1 (2017).
90. D. Mondal, B. Bhowmick, M.M.R. Mollick, D. Maity, N. Ranjan Saha, V. Rangarajan, D. Rana, R. Sen, and D. Chattopadhyay, *J. Appl. Polym. Sci.*, **131**, 1 (2014).